Lab on a Chip

PAPER

Cite this: *Lab Chip*, 2022, **22**, 1374

Shear and endothelial induced late-stage calcific aortic valve disease-on-a-chip develops calcium phosphate mineralizations†

Melissa Mendoza, [a] Mei-Hsiu Chen,[b] Peter Huang[c] and Gretchen J. Mahler*[a]

Received 15th October 2021,
Accepted 18th February 2022

DOI: 10.1039/d1lc00931a

rsc.li/loc

Calcific aortic valve disease (CAVD) is an active pathobiological process leading to severe aortic stenosis, where the only treatment is valve replacement. Late-stage CAVD is characterized by calcification, disorganization of collagen, and deposition of glycosaminoglycans, such as chondroitin sulfate (CS), in the fibrosa. We developed a three-dimensional microfluidic device of the aortic valve fibrosa to study the effects of shear stress (1 or 20 dyne per cm^2), CS (1 or 20 mg mL^{-1}), and endothelial cell presence on calcification. CAVD chips consisted of a collagen I hydrogel, where porcine aortic valve interstitial cells were embedded within and porcine aortic valve endothelial cells were seeded on top of the matrix for up to 21 days. Here, we show that this CAVD-on-a-chip is the first to develop human-like calcified nodules varying in calcium phosphate mineralization maturity resulting from high shear and endothelial cells, specifically di- and octa-calcium phosphates. Long-term co-culture microfluidic studies confirmed cell viability and calcium phosphate formations throughout 21 days. Given that CAVD has no targeted therapies, the creation of a physiologically relevant test-bed of the aortic valve could lead to advances in preclinical studies.

Introduction

Calcific aortic valve disease (CAVD) is an active pathobiological process ranging from mild valve thickening (aortic sclerosis) to severe leaflet calcification (aortic stenosis).[1–3] Late-stage CAVD has been characterized by increased leaflet stiffness due to the formation of calcified nodules, the disorganization of collagen bundles, and the deposition of glycosaminoglycans (GAGs), such as chondroitin sulfate (CS), in the fibrosa layer.[2,4] In the United States, it is reported that the prevalence of moderate to severe calcific aortic stenosis in patients ≥75 years old is 2.8% and is projected to more than double by 2050.[5] Current treatments for CAVD include surgical valve replacement and/or minimal drug interventions tailored to other cardiovascular diseases.[1] Advances in valve disease research have conventionally relied on animal and static cell culture models, but engineered dynamic models may help to further the understanding of CAVD onset and progression in a mechanically-complex environment. Organ-on-a-chip models, or microfluidic systems integrating living cells to mimic multicellular architectures and organ functional units, have emerged as tools to study tissue pathophysiology *in vitro*. Organ chips utilize engineering and cell biology to provide a mechanically-complex environment capable of recapitulating *in vivo* biological responses.[6]

The aortic valve is made up of three semilunar leaflets, each composed of three distinct layers characterized by their extracellular matrix (ECM) composition and orientation. The fibrosa layer is composed of circumferentially-aligned collagen fibers, the spongiosa is composed of collagen and randomly-oriented proteoglycans rich in GAGs, and the ventricularis is composed of mostly radially-orientated elastin. These layers are sandwiched between protective endothelial cell layers that provide mechanical strength, elasticity, and structural integrity to withstand various mechanical forces.[7,8] Leaflets are constantly exposed to shear, flexure, tension, and compression during each cardiac cycle, yet modelling this environment *in vitro* can be challenging due to their rapid, constant motion *in vivo*.[9–11] The calcific nodule-prone fibrosa is exposed to low (1 dyne per cm^2) oscillatory shear stress, while the ventricularis experiences high (20 dyne per cm^2) steady shear (Fig. 1a). Higher levels of shear stress on the fibrosa side have been reported in cases

[a] *Department of Biomedical Engineering, Binghamton University, P.O Box 6000, Binghamton, NY, 13902, USA. E-mail: gmahler@binghamton.edu; Tel: +1(607)777 5238*
[b] *Department of Mathematical Sciences, Binghamton University, Binghamton, NY, 13902, USA*
[c] *Department of Mechanical Engineering, Binghamton University, Binghamton, NY, 13902, USA*

† Electronic supplementary information (ESI) available: Supplementary methods and Fig. S1–S4. See DOI: 10.1039/d1lc00931a

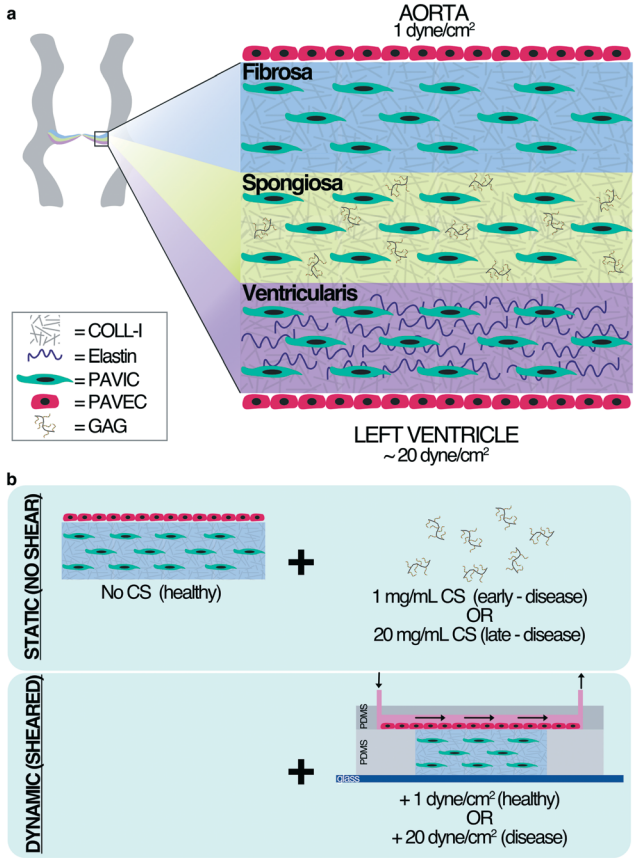

Fig. 1 Aortic valve anatomy and experimental comparison. a. Healthy aortic valve, leaflet microstructure, and native shear stresses. b. Experimental methods of static and dynamic aortic valve fibrosa model (COL-I = collagen-I, PAVIC = porcine aortic valve interstitial cells, PAVEC = porcine aortic valve endothelial cells, GAG = glycosaminoglycan, CS = chondroitin sulfate).

of aortic stenosis.[7] These forces are important in determining several biological responses, such as gene expression, protein activation, and changes in cell phenotype. Abnormal cardiac forces, specifically in CAVD pathogenesis, can induce ECM remodelling, alter cell proliferation and morphology, and initiate apoptosis, ultimately leading to disease initiation and progression within the fibrosa.[9,11–13]

Given the knowledge gaps in human CAVD pathophysiology, animal models emerged as vital tools in pre-clinical pharmacological studies. However, common CAVD animal models, such as mice, rabbits and pigs do not fully recreate human biological responses and/or require significant time and maintenance. Moreover, mice do not share human-like valve anatomy, rabbits cannot spontaneously develop atherosclerotic lesions, and pigs require long, expensive, and complex studies.[14]

Despite the myriad of pre-clinical and clinical valve studies, many details of the human CAVD pathological cascade remain unknown. Healthy and viable human aortic valve leaflet tissue is not realistic to obtain given that most are from valve replacement surgeries. However, similar to that of human physiology, pigs develop atherosclerotic vascular and valvular sclerosis when fed high-fat and high-cholesterol diets for 2 weeks to 6 months, and have trilayer leaflets and comparable anatomical structure.[14,15] Further, porcine interstitial and endothelial cells are commonly used for *in vitro* valve models due to well-established isolation protocols and tissues are more readily-accessible than healthy human tissue.[2,12,14,16] *In vitro* models further explore human/porcine similarities and allow study timelines to shorten from 3–8 months in animal models to 2–21 days in benchtop models.[14] Several research groups have developed static two-dimensional (2D) and three-dimensional (3D) aortic valve models utilizing different approaches, such as transwells, novel biomaterials, and bioengineered or natural hydrogels. Gould *et al.* utilized porcine aortic valve interstitial cells (PAVIC) and porcine aortic valve endothelial cells (PAVEC) embedded into a poly(ethylene glycol)/transwell platform to identify various co-culture signalling pathways for up to 9 days.[17] Tseng *et al.* developed a 3D PAVIC + PAVEC co-culture assembly using magnetic levitation to study cell phenotypes and ECM production over 3 days.[18] Hjortnaes *et al.* induced endothelial-to-mesenchymal transformation (EndMT) with transforming growth factor beta-1 (TGFβ-1) and osteogenic medium in transwells to study the interaction between ovine aortic valve endothelial and interstitial cells over 14 days.[19] A separate study by Hjortnaes *et al.* combined methacrylated gelatin and hyaluronic acid to form a 3D hydrogel platform to study PAVIC phenotypic fate as a response to substrate stiffness and TGFβ-1 in 21 days.[20] Dahal *et al.* utilized collagen I(COL-I)-GAG hydrogels with PAVEC to identify the role of EndMT in both early- and late-stage CAVD in 48-hour cultures.[4] Most recently, Gee *et al.* developed a mechanically-constrained COL-I hydrogel embedded with PAVIC and/or PAVEC to study their intercellular communication *via* paracrine signalling over 7 days.[21]

While static *in vitro* models of the aortic valve have emerged as alternatives to animal models, valves are mechanically complex and a dynamic environment is needed to study valvular mechanobiology. There have been few research groups to study aortic valve disease *in vitro* under dynamic conditions. In 2006, Butcher *et al.* applied continuous steady shear (20 dyne per cm^2) for 48 hours in a parallel plate flow system to study valvular and vascular hemodynamics.[22] Furthermore, Butcher and Nerem studied the effects of shear stress on a 3D PAVIC + PAVEC co-culture model for up to 96 hours.[23] Young *et al.* developed a microfluidic device to compare cell–ECM interactions between PAVEC and vascular endothelial cells under 11–220 dyne per cm^2 steady shear for 4, 8, and 12 minute intervals.[24] Chen *et al.* developed a methacrylated gelatin/bilayer membrane device to model PAVIC + PAVEC paracrine interactions over 24 hours under 20 dyne per cm^2 steady shear.[25] Mahler *et al.* characterized the role of shear stress on EndMT in a 3D microfluidic bioreactor utilizing PAVEC exposed to shear (2, 10, and 20 dyne per cm^2) over 48 hours.[26] Wang *et al.* developed an organ-on-a-chip device to study the application of mechanical stimulation (0–4.26 dyne

per cm^2) on PAVIC transformation throughout 4 days.[27] Most recently, in 2018, Lee *et al.* explored the mechanobiological response of PAVEC under shear stress (up to 20 dyne per cm^2) and frequency profiles (0.8–2 Hz) within a microfluidic generator throughout 24 and 48 hours.[28] Still, there is room for further exploration and innovation in the field of aortic valve microfluidics to model valvular diseases and expand pre-clinical tools. Physiologically-relevant dynamic valve models have the potential to elucidate the pathophysiology of human CAVD.

Here, we developed a 3D microfluidic device of the aortic valve fibrosa layer capable of cell culture for up to 21 days to study the effects of shear stress, endothelial cells, and chondroitin sulfate on *in vitro* calcification. We assessed the hypothesis that culture calcification will increase with endothelial cell presence, high chondroitin sulfate concentration, and high shear rates. This hypothesis was tested by comparing static (no shear) and dynamic (1 or 20 dyne per cm^2 shear stress) 3D hydrogel cultures *via* (1) qualitative and quantitative Alizarin Red S staining analysis, (2) scanning electron microscopy with energy dispersive X-ray spectroscopy analysis, and (3) long-term culture viability.

Experimental

Materials and methods

CAVD on-a-chip devices were fabricated using soft lithography and corona discharge, and contain an internal 3D hydrogel matrix. Disease progression was assessed using Alizarin Red S and scanning electron microscopy with energy dispersive X-ray spectroscopy, and culture viability was examined with confocal microscopy. The following sections provide detailed Materials and methods.

Microchannel fabrication

Detailed methods are provided in ESI.†

Device design

The polydimethylsiloxane (PDMS) (Sylgard-184, Dow Corning) devices consisted of a flow channel (30 mm × 15 mm × 50 μm), and an internal cylindrical reservoir (6 mm diameter × 3 mm) for containing a 3D matrix. Mina *et al.* previously characterized the computational fluid dynamics within this microchannel.[29] Detailed methods are provided in ESI.†

Primary cell culture

All models utilized PAVIC and/or PAVEC isolated from tissues obtained at local abattoirs, as described in Gould and Butcher.[16] PAVIC (passage 3) were grown to confluency in Dulbecco's modified Eagle medium (DMEM) (Gibco Life Tech) supplemented with 10% fetal bovine serum (FBS) (VWR) and 1% penicillin–streptomycin (Gibco Life Tech). PAVEC (passages 3–5) were grown to confluency in a 50 μg mL^{-1} COL-I-coated (Corning) flask in DMEM supplemented with 10% FBS, 1% penicillin–streptomycin, and 50 U mL^{-1} heparin sulfate (Sigma-Aldrich) prior to seeding experiments.

Hydrogel fabrication

The 3D ECM was made by mixing a PAVIC pellet at 1×10^6 cells per mL with sterile 3XDMEM, 18 MΩ water, FBS, 0.1 M sodium hydroxide (Sigma-Aldrich), and rat-tail COL-I (Corning) on ice. Hydrogels consisted of 1.5 mg mL^{-1} COL-I-only healthy controls or 1.5 mg mL^{-1} COL-I with CS (Sigma-Aldrich) (early-disease = 1 mg mL^{-1} or late-disease = 20 mg mL^{-1}). In static conditions, PAVIC-embedded 300 μL hydrogels were seeded into 50 μg mL^{-1} Cell-TAK™ pre-treated (Corning) 24-well plates (Corning). After 1 hour, PAVEC were seeded onto the matrix at 95 000 cells per cm^2 in 400 μL PAVIC medium, and medium was replaced every 48 hours. In dynamic conditions, the PAVIC-embedded (1×10^6 cells per mL) hydrogel was injected into the pre-treated PDMS middle layer utilizing a 23G sterile needle (BD) and allowed to crosslink for 1 hour. PAVEC (95 000 cells per cm^2) were introduced onto the matrix *via* microchannel inlet and allowed to attach for 4 hours prior to the flow initiation. Each device was then connected to a peristaltic pump (205S, Watson Marlow) using 0.51 mm inner diameter tubing (Cole-Palmer) and 0.79 mm inner diameter connector tubing (Cole-Palmer). Steady shear stresses of 1 or 20 dynes per cm^2 were applied to the top of the matrix by controlling the flow rate. A recirculating 500 μL reservoir of PAVIC medium was replenished every 48 hours. Static and dynamic conditions were placed at 37 °C and 5% CO_2 for up to 21 days (Fig. 1b).

Alizarin Red S (ARS) staining

Disease progression was assessed following experimentation with ARS (Sigma-Aldrich), a histological stain for calcium deposition.[30–32] Static and dynamic hydrogels were washed 3 times with 1× phosphate buffered saline (PBS) (10× PBS Ultrapure, VWR), fixed with 4% paraformaldehyde (PFA) (Sigma-Aldrich) in 1× PBS overnight at 4 °C, washed again 3 times with 1× PBS, and stained with 40 mM ARS (pH 4.1–4.3) for 20 minutes using gentle agitation.[26] Unbound ARS stain was removed with 18 MΩ water washes and gentle agitation till all unbound dye was removed from hydrogels. Brightfield images (Eclipse Ts2, Nikon) were obtained and used to quantify nodule areas and pixels stained in ImageJ.[33] Nodule area quantification was obtained using measurement tools to identify the surface area of individual nodules. Additionally, the percent-stained area was quantified: images were converted to 16-bit, converted to binary using a threshold to distinguish the background (black pixels) from calcified nodules (white pixels), and obtained the percent-stained area per image with the particle analysis tool. Image quantifications represented as $n \geq 4$ images per condition. Bound ARS stain was then released from hydrogels with 10% acetic acid (Amresco) in 18 MΩ water overnight using gentle agitation, submerged in a bath sonicator for 1 hour, heated for 10 minutes at 85 °C, placed on ice for 5 minutes and

centrifuged at 19357 × *g* for 15 minutes. The supernatant was neutralized with 10% ammonium hydroxide (Sigma-Aldrich) in 18 MΩ water and absorbance was read at 405 nm using Gen5™ (BioTek) with a plate reader (Synergy H1, BioTek), where ARS concentration was calculated using a standard curve.[31,32] All conditions contained $n \geq 3$ hydrogels, where each dynamic data point represents a microfluidic device and each static data point represents average per experiment.

Scanning electron microscopy with energy dispersive X-ray (SEM/EDX) spectroscopy

Disease progression was also assessed with SEM/EDX, an imaging and spectroscopy technique to analyze microstructure and chemical composition.[34–37] Following 3–21 days, static and dynamic hydrogels were washed 3 times with 1× PBS, fixed with 4% PFA overnight, and washed again 3 times with 1× PBS. Samples were subjected to ethanol (Koptec) dehydration for 20 minutes each: 50%, 70%, 95%, and 100% ethanol in 18 MΩ water, and again 100% ethanol in 18 MΩ water. Samples were then subjected to hexamethyldisilazane (HMDS) (Sigma-Aldrich) dehydration for 20 minutes each: 1 : 2 HMDS : 100% ethanol, 2 : 1 HMDS : 100% ethanol, 100% HMDS and again 100% HMDS overnight till the sample dried out in the fume hood.[35,37] Samples were mounted onto aluminum sample holders with carbon tape (Electron Microscopy Sciences) and prepared with 15 nm carbon coat (Cressington 208C, Ted Pella). Samples were imaged under SEM (FE-SEM Supra-55 VP, Zeiss) with the following parameters: 3–5 kV, 6–8 mm working distance, and the In-Lens detector. EDX analyses were performed with the following SEM and software (EDAX GENESIS v5.11, Ametek) parameters: 15 kV, 8.5 mm working distance, and 12.5–51.2 μs Amp Time to ensure 10–40% dead time. Data represented as $n \geq 5$ measurements per condition in atomic percent (At%) and calculations of At% calcium to phosphorous ratios (Ca/P) were used to quantify calcium phosphate mineralizations.

Viability assessment

Static and dynamic cultures were observed throughout 21 days to assess cell morphology and long-term viability. After days 3, 7, 14, or 21, hydrogels were washed 3 times with 1× PBS, stained with 3 μM calcein AM (488/520 nm, Thermo Fisher) for 30 minutes at 37 °C and 5% CO_2, and imaged utilizing confocal laser scanning microscopy (LSM 880, Zeiss). Images were further used to assess cell area and circularity at 14 and 21 days; detailed methods are provided in ESI.†

Statistical analysis

All data was presented as mean ± standard error of the mean (SEM), where analyses were conducted in GraphPad Prism 8 (GraphPad). The Kruskal–Wallis tests with Dunn's multiple comparisons *post-hoc* tests were used to compare groups, where p-value < 0.05, was considered statistically significant. Experimental sample sizes (n) were specified in methods and figure legends.

Results & discussion

Results

Shear stress and endothelial cells drive microfluidic derived calcification in 14 days. Microfluidic devices were used in 14 day studies with PAVIC-only embedded into COL-I hydrogel constructs and demonstrated minimal calcification, as seen in qualitative and quantitative ARS results (Fig. 2 and 3 and S1†). ARS stain concentration increased in the presence of increasing shear compared to static controls (Fig. 3a–c). In the presence of either 1 or 20 mg mL^{-1} CS, average nodule area decreased in dynamic environments (Fig. 3d–f). Additionally, regardless of GAG concentration, total average percent-stained area increased in the presence of shear stress compared to that of static controls (Fig. 3g–i). To further enhance the aortic valve fibrosa model and determine the role of endothelial cells, PAVEC were seeded onto the 3D constructs for 14 day studies. Co-culture models likewise demonstrated that increased shear stress resulted in increased calcification (Fig. 2 and 4 and S1†). As seen in ARS qualitative results, there was an increase in calcified nodules present in dynamic conditions compared to static models and interstitial cell-only cultures (Fig. 2 and S1†). Quantitatively, ARS concentration increased as shear stress increased, regardless of the GAG concentration in the culture (Fig. 4a–c). In the presence of both 1 or 20 mg mL^{-1} CS, surface area analysis of nodule size indicated that the average nodule area decreased with shear stress (Fig. 4d–f). Similar to that of ARS stain quantification, the total percent-stained area in qualitative analysis indicated that increased shear also resulted in increased stained area regardless of CS concentration (Fig. 4g–i). Although individual nodule areas were smaller in dynamic conditions, they constituted a larger percent-stained area (Fig. 2–4).

SEM/EDX reveals calcified nodule microstructure and presence of calcium phosphate mineralizations. SEM/EDX spectroscopy was used to support ARS results. Given results of high GAG content (20 mg mL^{-1} CS) and high shear stress (20 dyne per cm^2) combined, this study explored nodule formation under SEM compared to their static counterparts. Calcified nodule microstructure showed mineral structures embedded within the fibrous COL-I matrix, specifically localized around fiber bundles (Fig. 5a). EDX analysis revealed the presence of several elements including: carbon, nitrogen, oxygen, sodium, magnesium, aluminum, silicon, phosphorous, sulfur and calcium (Fig. 5b, c and 6). Given the elements of interest in calcification studies, EDX analyses demonstrated At% for calcium, phosphorous, magnesium, and aluminum. Results indicated higher calcium and phosphorous At% in dynamic hydrogels compared to static controls, and significantly higher percentages in co-culture samples compared to those with PAVIC-only (Fig. 5b and d). Elemental percentages for each condition, including

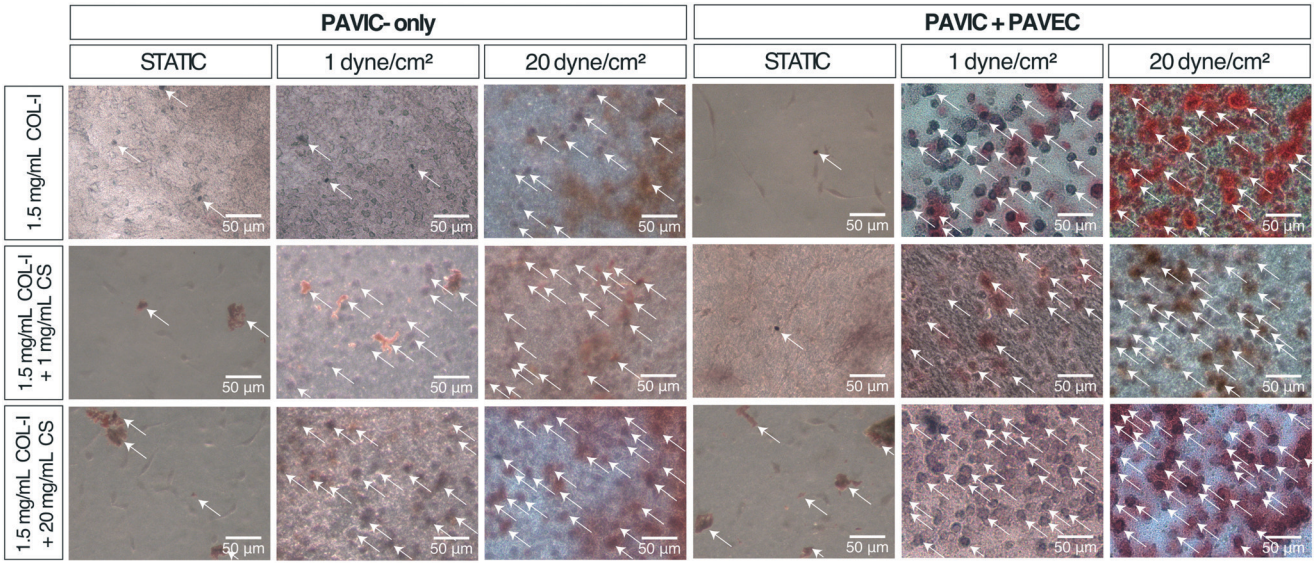

Fig. 2 Static and microfluidic Alizarin Red S (ARS) staining after 14 days, porcine aortic valve interstitial cells (PAVIC) only and when co-cultured with porcine aortic valve endothelial cells (PAVEC). ARS qualitative images, arrows indicate calcific nodules (scale = 50 μm). Magnified high shear conditions (scale = 200 μm) shown in Fig. S1† (COL-I = collagen-I, PAVIC = porcine valve interstitial cells, PAVEC = porcine aortic valve endothelial cells, CS = chondroitin sulfate).

magnesium and aluminum trace elements, were further compared (Fig. S2†). Ca/P ratios, demonstrating the level of mineralization, were plotted to show each measurement against a variety of well-studied pathobiological calcium phosphates with increasing maturity leading to hydroxyapatite (Ca/P = 1.67) formation. Results indicated that dynamic-derived calcified nodules were composed of several forms of naturally-occurring calcium phosphates (Fig. 5d and e). In PAVIC-only studies, Ca/P ratios aligned with dicalcium phosphates (Ca/P = 1) where Ca/P = 1.13 ± 0.04 at high shear and Ca/P = 1.08 ± 0.12 when combined with high CS (Fig. 5d). In PAVIC + PAVEC studies, Ca/P ratios aligned with dicalcium phosphates and octacalcium phosphates (Ca/P = 1.33) where Ca/P = 1.24 ± 0.03 at high shear and Ca/P = 1.14 ± 0.02 when high shear was combined with high CS. However, static Ca/P ratios were statistically different and fell below all the calcium phosphate thresholds: PAVIC-only Ca/P = 0.06 ± 0.02, PAVIC + 20 mg mL^{-1} CS Ca/P = 0.10 ± 0.03, and PAVIC + PAVEC Ca/P = 0.09 ± 0.03, PAVIC + PAVEC + 20 mg mL^{-1} CS Ca/P = 0.17 ± 0.04 (Fig. 5d and e).

Long-term co-culture microfluidic studies confirm cell viability and calcium phosphate formations. Given the intensity of the calcification forming as a result of dynamic conditions, cell viability and morphology was assessed. Results indicated that both static and microfluidic cultures were viable for up to 21 days, as shown *via* live 3D Calcein AM staining. While cells embedded into static hydrogels began to spread throughout the matrix, cells embedded into dynamic hydrogels at 20 dyne per cm2 had a significantly higher circularity index and did not spread throughout the matrix (Fig. 6a and S3†). Further, formation of calcium phosphates over long-term cultures for PAVIC + PAVEC at 20 dyne per cm^2 and 20 mg mL^{-1} CS was analyzed. At 14 and 21 days, cultures showed the same elemental spectra with varying intensity and comparable mineral microstructure (Fig. 6b). This demonstrated that although the calcium and phosphorous At% were significantly higher at 21 days, the Ca/P ratios were not statistically different to those of 14 day studies with the same culture conditions (PAVIC + PAVEC at high shear and high CS 21 day culture Ca/P = 1.15 ± 0.01) (Fig. 6b and c). Additionally, dynamic Ca/P ratios from days 7–21 aligned with dicalcium phosphate and octacalcium phosphate minerals, while static Ca/P ratios aligned with monocalcium phosphates (Ca/P = 0.5) (Fig. 6c). SEM images indicated microcalcifications as early as 3 days under high shear embedded into COL-I fibrous bundles, yet Ca/P ratios lacked mineral maturity (Fig. 6c and S4a†). Static and dynamic calcium and phosphorous elemental percentages were compared at each time point up to 21 days (Fig. S4b and c†).

Discussion

Few studies have employed the use of dynamic *in vitro* models to study aortic valve mechanobiology.[22–28] In this study, a multi-layer PDMS microfluidic device capable of viable 3D cell culture for up to 21 days at high shear was developed. To our knowledge, this is the first microdevice to develop highly-calcified cultures mainly driven by high shear and endothelial cell presence. Natural biopolymer-based 3D hydrogels, such as COL-I hydrogels, provide physiologically-relevant cell culture environments, matrix tunability, and microstructural complexity.[4,7,20] COL-I is also the most abundant collagen type in the aortic valve by dry weight (74%), in comparison to collagen-III (24%) and collagen-V (2%).[38] CS was integrated into the COL-I hydrogels to mimic

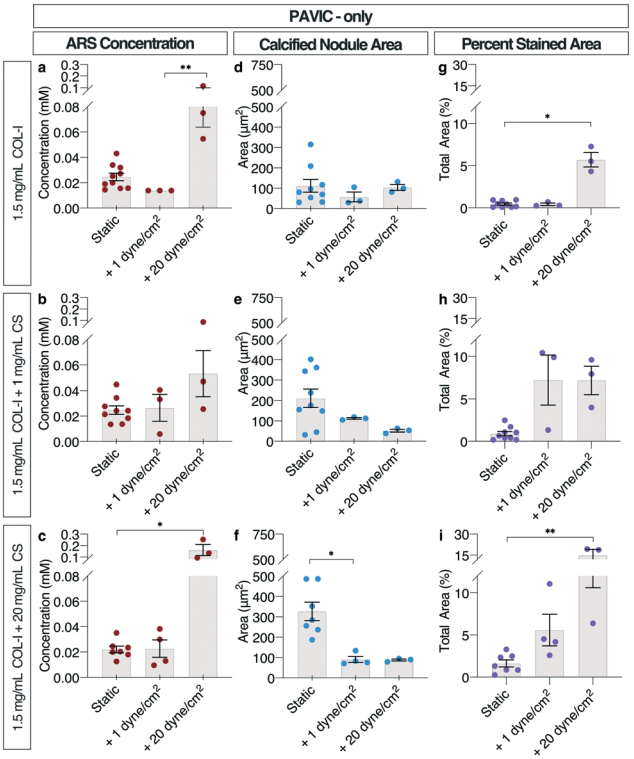

Fig. 3 Static and microfluidic Alizarin Red S (ARS) staining quantification after 14 days, porcine aortic valve interstitial cells (PAVIC) only. ARS stain quantification static and dynamic a. without chondroitin sulfate (CS), b. with 1 mg mL^{-1} CS, c. with 20 mg mL^{-1} CS. Mean ± SEM, $n \geq 3$ experiments/condition. ARS average nodule area quantification static and dynamic d. without CS, e. with 1 mg mL^{-1} CS, f. with 20 mg mL^{-1} CS. ARS average percent-stained area quantification static and dynamic g. without CS, h. with 1 mg mL^{-1} CS, i. with 20 mg mL^{-1} CS. Mean ± SEM, $n \geq 4$ images/condition. Statistical significance shown according to Kruskal–Wallis with Dunn's multiple comparisons *post-hoc* test, *$p < 0.05$ **$p < 0.01$ (COL-I = collagen-I, PAVIC = porcine valve interstitial cells, CS = chondroitin sulfate).

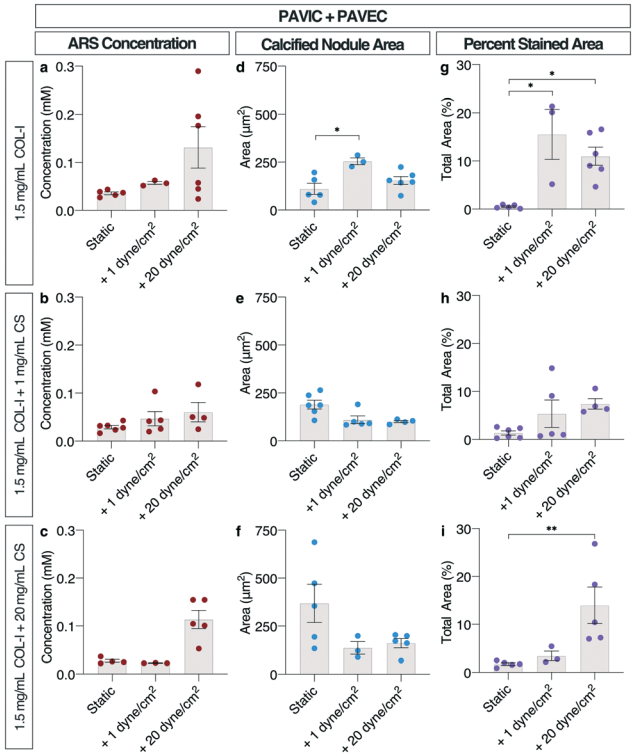

Fig. 4 Static and microfluidic Alizarin Red S (ARS) staining after 14 days, co-cultured porcine aortic valve interstitial cells (PAVIC) and porcine aortic valve endothelial cells (PAVEC). ARS stain quantification static and dynamic a. without chondroitin sulfate (CS), b. with 1 mg mL^{-1} CS, c. with 20 mg mL^{-1} CS. Mean ± SEM, $n \geq 3$ experiments/condition. ARS average nodule area quantification static and dynamic d. without CS, e. with 1 mg mL^{-1} CS, f. with 20 mg mL^{-1} CS. ARS average percent-stained area quantification static and dynamic g. without CS, h. with 1 mg mL^{-1} CS, i. with 20 mg mL^{-1} CS. Mean ± SEM, with $n \geq 4$ images/condition. Statistical significance shown according to Kruskal–Wallis with Dunn's multiple comparisons *post-hoc* test, *$p < 0.05$ **$p < 0.01$ (COL-I = collagen-I, PAVIC = porcine valve interstitial cells, PAVEC = porcine valve endothelial cells, CS = chondroitin sulfate).

the migration of proteoglycans that deposit around calcified nodules in the fibrosa during CAVD.[2,4] Previous studies indicate that high levels of CS contribute to the highest rates of EndMT and disease progression when compared to other GAGs, such as hyaluronic acid and dermatan sulfate.[4,29,39] Although the results shown in this study indicate that shear and endothelial cells play a larger role in driving disease progression, 20 mg mL^{-1} CS did also influence the outcomes.

It was evident that endothelial cells played a major role in the promotion of culture calcification in both static and dynamic models. However, there are conflicting studies referring to the influence of valvular endothelial cells on interstitial cell activation. Studies have demonstrated that the presence of PAVEC suppress and protect against culture calcification, and thereby model valve homeostasis.[22,23,25,26,17,19] However, recent studies such as Gee *et al.* align with the current findings, reporting that PAVEC actively induce PAVIC pathological remodelling and calcification *via* paracrine signaling.[21] Further, although Hjortnaes *et al.* showed that ovine aortic valvular interstitial cells suppress endothelial calcification, in the same study they also showed that in transwell co-cultures, endothelial cells further contributed to interstitial cell myofibroblastic activation and calcification.[19] These studies indicate that endothelial dysfunction and EndMT play a role in valvular pathophysiology, leading to disease onset and progression. EndMT, a process well-studied in valvular development, is a process by which endothelial cells undergo phenotypic and functional changes thereby lose endothelial cell markers (CD31/PECAM-1) and gain mesenchymal cell markers (αSMA), and migrate into the interstitial space.[4,8,21,26,29] Rattazzi and Pauletto questioned whether endothelial cells have a double-faced behavior leading to the complexity of valve calcification; a paracrine negative feedback loop may be driving interstitial and/or endothelial cell activation and calcification.[40] This could explain the conflicting literature, stressing that future studies continue to identify interstitial–endothelial interactions and the role that EndMT plays throughout CAVD initiation and progression.

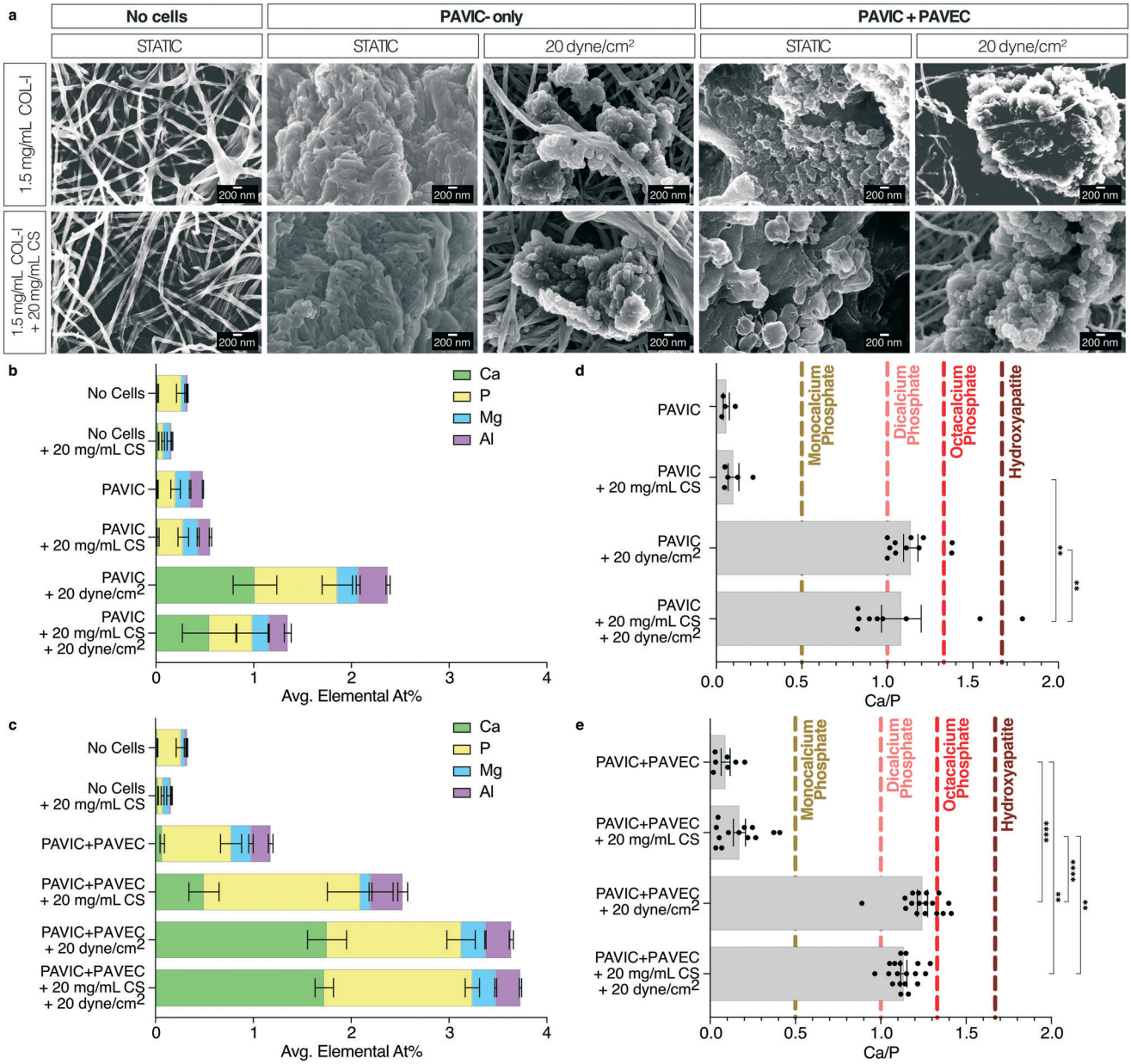

Fig. 5 Static and microfluidic scanning electron microscopy with energy dispersive X-ray spectroscopy (SEM/EDX) after 14 days, porcine aortic valve interstitial cells (PAVIC) only and when co-cultured with porcine aortic valve endothelial cells (PAVEC). a. SEM qualitative images (scale = 200 nm). EDX qualitative elemental atomic percentages in b. PAVIC-only and c. PAVIC + PAVEC cultures. Mean ± SEM, $n \geq 5$ measurements. Statistical significance shown in Fig. S2.† Calcium phosphate mineralization based on EDX atomic percentages in d. PAVIC-only and e. PAVIC + PAVEC co-cultures, where monocalcium phosphate calcium to phosphate ratio (Ca/P) = 0.5, dicalcium phosphate Ca/P = 1.0, octacalcium phosphate Ca/P = 1.33, and hydroxyapatite Ca/P = 1.67. Mean ± SEM, $n \geq 4$ calculations. Statistical significance shown according to Kruskal–Wallis with Dunn's multiple comparisons *post-hoc* test, $*p < 0.05$ $**p < 0.01$ $***p < 0.001$ $****p < 0.0001$ (COL-I = collagen-I, PAVIC = porcine valve interstitial cells, PAVECs = porcine valve endothelial cells, CS = chondroitin sulfate, Ca = calcium, P = phosphorous, Mg = magnesium, Al = aluminum, Ca/P = calcium to phosphorous ratio, At% = atomic percent).

As seen in this study and within current literature, valvular disease is an active procalcific process, leading to severe extracellular matrix remodelling, fibrosis, and calcification.[3,8,13] Experimental CAVD models *in vitro*, *ex vivo*, and *in vivo* have identified signalling pathways to elucidate molecular mechanisms for this active process, and to provide potential diagnostic and therapeutic outcomes.[41] Bone morphogenic protein (BMP), Notch1, wingless-related integration site (Wnt), and TGFβ1 signalling pathways have been found to play a role in CAVD pathophysiology, specifically driving endothelial cell dysfunction promoting interstitial osteogenic differentiation.[41–47] Similarly, studies have shown that EndMT is dependent on BMP, Notch, Wnt, and TGFβ signalling.[46] Ankeny *et al.* identified SMAD-1/5/8 phosphorylation and BMP-2/4/6 expression in *ex vivo* human calcified fibrosa tissue.[42] Sucosky *et al.* demonstrated that in response to aortic pulsatile

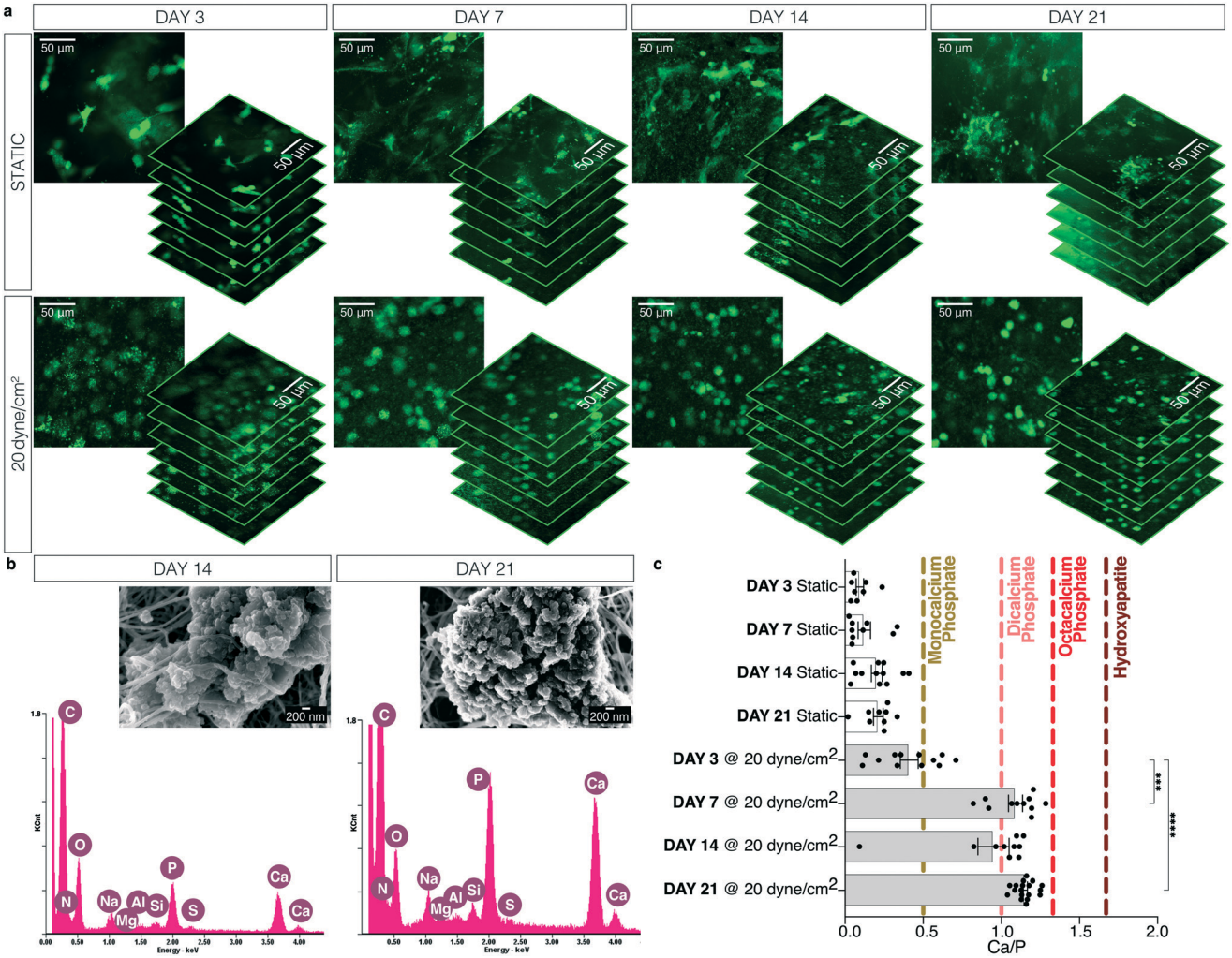

Fig. 6 Static and microfluidic viability and calcium phosphate mineralization throughout 21 days, porcine aortic valve interstitial cells (PAVIC) co-cultured with porcine aortic valve endothelial cells (PAVEC) and 20 mg mL^{-1} chondroitin sulfate (CS). a. Static and high shear 20 dyne per cm^2 qualitative viability *via* Calcein AM days 3, 7, 14 and 21 (representative 2D images and z-slices 4 μm apart, scale = 50 μm). Cell area and circularity was quantified at days 14 and 21 in Fig. S3.† b. Scanning electron microscopy (SEM) at 14 and 21 days (scale = 200 nm) and energy dispersive X-ray spectroscopy (EDX) spectra output. All SEM images shown in Fig. S4.† c. Calcium phosphate mineralization based on EDX atomic percentages, where monocalcium phosphate calcium to phosphate ratio (Ca/P) = 0.5, dicalcium phosphate Ca/P = 1.0, octacalcium phosphate Ca/P = 1.33, and hydroxyapatite Ca/P = 1.67. EDX elemental atomic percentages for calcium and phosphorous shown in Fig. S4.† Mean ± SEM, $n \geq 4$ calculations. Statistical significance shown according to Kruskal–Wallis with Dunn's multiple comparisons *post-hoc* test, $*p < 0.05$ $**p < 0.01$ $***p < 0.001$ $****p < 0.0001$ (C = carbon, N = nitrogen, O = oxygen, Na = sodium,Mg = magnesium, Al = aluminum, Si = silicon, P = phosphorous, S = sulfur, Ca = calcium, Ca/P = calcium to phosphorous ratio).

shear stress for 48 hours, cultures of porcine aortic valve leaflets expressed BMP-4.[43] Studies have shown that TGFβ supplementation of *in vitro* and *ex vivo* systems induces nodule formation and EndMT.[12,26,29,41,47] Gaur *et al.* proposed that the Wnt/β-catenin pathway drives osteoblastic differentiation, similar to that of BMP and TGFβ by RUNX2 activation.[44] Garg *et al.* established that the Notch1 pathway mutations, requiring cell–cell contact, induce CAVD.[45] Although not directly investigated here, BMP, Notch, Wnt, and TGFβ signalling may be at play in this *in vitro* calcification process.

Shear stress was hypothesized to be a driving factor for calcification, given that abnormal hemodynamic forces have been known to cause tissue remodeling.[7,9,11] In this model, diseased conditions were represented by high 20 dyne per cm^2 shear, while healthy conditions were represented by 1 dyne per cm^2 shear stress as normally experienced by the fibrosa. Some *in vitro* dynamic studies have reported that the introduction of shear stress resulted in a homeostatic response.[22,23,25,26] Butcher *et al.* showed that the presence of 20 dyne per cm^2 over 48 hours had a protective effect on PAVEC against calcification.[22] Chen *et al.* demonstrated that PAVEC significantly suppressed PAVIC myofibroblastic activation within a 3D culture over 24 hours, which was then further enhanced by the presence of 20 dyne per cm^2 steady shear.[25] Mahler *et al.* detailed that PAVEC exposed to 2 dyne per cm^2 or oscillatory shear over 48 hours upregulated

EndMT and inflammation, and did not when exposed to higher shear (10 or 20 dyne per cm^2).[26] Butcher and Nerem found that 20 dyne per cm^2 for 96 hours on a PAVIC + PAVEC co-culture model allowed PAVEC to stimulate PAVIC into a quiescent phenotype. However, that same study demonstrated that PAVIC-only cultures exposed to the same shear increased cell activation.[23] Similarly, Wang *et al.* found that 2D cultures exposed up to 4.26 dyne per cm^2 steady shear enhanced PAVIC myofibroblastic transformation.[27] Further, PAVEC-only cultures exposed to steady shear expressed pathological differentiation markers over 48 hours.[28] Again, there are discrepancies in literature with respect to PAVIC-only, PAVEC-only, and PAVIC + PAVEC activation as a response to dynamic conditions. It is also important to note that published studies aforementioned identified cell–cell and cell–ECM changes only up to 4 days under shear. Although prior studies set the groundwork for dynamic valvular research, it is possible that these studies may not fully align with the findings in this study due to their short-term culture periods. This study pushes the late-stage valvular research field to create long-term, shear-induced pathobiological changes in physiologically-relevant 3D co-cultures. Abnormally high shear stresses within this fibrosa model could induce changes in the ECM and the cells, specifically causing apoptosis.[9,11] SEM images showed that nodules were formed around and embedded into COL-I bundles as early as 3 days at high shear, whereas static micrographs of the matrix show the random distribution of COL-I fibers. This demonstrates engineered calcification disrupting the ECM into dense COL-I bundles, yet further work is need to quantify these changes within the microfluidic system. Additionally, changes in cell morphology as a result of high shear were shown, while also observing a large population of viable cells throughout long-term cultures. Studies have shown microcalcifications to occur at sites of cell death, whether through apoptosis or necrosis, and thereby considering cytoskeletal remains as a mechanism for calcium accumulation.[8] However, Rodriguez and Masters found not only apoptotic and necrotic cells localized around nodules, but also found a strong majority of viable cells.[48] This indicates that apoptotic and necrotic cell presence is still not well understood in calcification studies.[8]

ARS has been conventionally used to histologically identify calcification, yet the ARS stain is not highly-specific and depends on the pH and concentration. In 1968, Puchtler *et al.* showed that ARS binds to calcium deposits intensely or selectively to varying minerals at different pH levels, leading to differences in histological color.[30] After cross-examination of Puchtler *et al.* with results in this study, imaging hinted at the possible traces of calcium, magnesium, iron, phosphorous, copper, sulfates, and hydroxides.[30] However, further identification was needed to evaluate calcific nodule formation. SEM/EDX has increasingly been used for biological samples to analyze chemical composition, composition distribution, and composition concentration of a sample.[31,34–37] Here, SEM was used to confirm mineralization and EDX to assess the elemental composition of those nodules, and urge that future studies rely on SEM/EDX to identify pathobiological calcification.

Although substantial nodule formation within 14 days was shown without the need for osteogenic medium, FBS- and glucose-rich basal medium could be contributing to cell activation towards disease. Landry *et al.* identified that the addition of increased nutrient content, such as serum exceeding 2% or high glucose (>10 mM), and mechanical stimuli promote the activation of quiescent primary cardiac fibroblast.[49] Similarly, a static PAVIC calcification study utilized low serum (1% FBS) for calcification studies to isolate the effects of cell–ECM interactions.[48] Further investigation is needed to isolate the effects of nutrient content from cell–cell signalling and cell–ECM calcification studies.

Hydroxyapatites (Ca/P = 1.67) are common mineralizations found in the pathological deposition of minerals and organic compounds of diseases such as cancer, cardiovascular abnormalities, and osteoporosis.[31,37,50] As seen in *ex vivo* studies of human calcified aortic valves, the microfluidic device-derived calcifications are similarly composed of a variety of naturally-occurring calcium phosphates: monocalcium phosphates (Ca/P = 0.5), dicalcium phosphates (Ca/P = 1), and octacalcium phosphates (Ca/P = 1.33). Mineralization studies identify mono-, di-, and octa-calcium phosphates as the main calcium phosphate phases and precursors to hydroxyapatite formation, where the formation highly depends on pH, temperature, and culture conditions.[35,51,52] Although hydroxyapatite mineralizations were not found, there were several measurements relevant to dicalcium phosphates and octacalcium phosphates in highly-calcified conditions. Studies of mineralized tissue and pathological calcifications consider that the presence of hydroxides and stable magnesium complexes are favorable for the formation of calcium phosphate precipitations, which can explain the detection of such trace elements in these EDX studies. Trace elements, where At% is <1%, have the ability to influence the reactivity and stability of biologically-formed mineralizations, specifically the solubility and microstructural changes.[50] Culture time was further assessed as a factor for mineral maturity, but 21 day dynamic co-cultures at high shear and high CS were not sufficient to produce hydroxyapatites.

Given the complexity of CAVD, it is possible that the introduction of external stimuli, such as oxidized low-density lipoproteins, inflammatory cytokines (ex. TGFβ-1 or tumor necrosis factor alpha (TNFα)), and/or osteogenic medium, may further lead to hydroxyapatite formation.[2,11,19,29,36,53] Additional complexity that could advance the model includes the incorporation of complex hemodynamic forces exhibited *in vivo* (ex. laminar *versus* turbulent flow, steady *versus* pulsatile *versus* oscillatory flow),[9–11,26,28,43] and further microstructural complexity, such as the incorporation of a three-layer system comprising of the fibrosa, spongiosa, and ventricularis,[8,54] or the incorporation of oxidized low-density lipoproteins and immune cells to further progress the model toward a pathological cascade.[13,41,53]

Conclusions

A microfluidic device capable of withstanding high-shear with viable cell cultures for up to 21 days has been developed, where cultures produced human-like calcified nodules varying in calcium phosphate mineralization maturity. The key takeaways of this study include: 1) development of a 3D microfluidic late-stage CAVD modelling platform, 2) creation of human-like calcified nodules of varying calcium phosphate maturity as those seen in *ex vivo* calcified human aortic valves, 3) significant calcification generated in a 14 day time frame, and 4) no external stimuli, such as osteogenic medium or inflammatory cytokines, needed to drive disease. This research may provide key answers to hypothesized pathways leading to CAVD onset and progression. Although this first late-stage CAVD-on-a-chip model requires further development, there is no current targeted treatment for CAVD aside from total valve replacement and this model is progress toward a physiologically-relevant test-bed of the aortic valve fibrosa for preclinical toxicology and pharmacology applications.

Author contributions

M. M., M. C., P. H., and G. J. M. conceptualized research goals and aims, and secured funding. M. M. performed all investigations and collected data. M. M and M. C. conducted formal data analysis. P. H. and G. J. M. contributed resources, materials, and tools. M. M. and G. J. M. wrote the manuscript. M. M., M. C., P. H., and G. J. M. reviewed and edited the manuscript.

Conflicts of interest

There are no conflicts to declare.

Acknowledgements

This work is supported by National Science Foundation (NSF) #1919438 (G. J. M./P. H./M. C.), American Heart Association (AHA) Predoctoral Fellowship #20PRE34990041 (M. M.), Clifford D. Clark Diversity Fellowship (M. M.), and LSAMP Bridge to Doctorate (M. M.). The authors would like to acknowledge staff at Binghamton University's Nanofabrication Laboratory (NLB), Analytical and Diagnostics Laboratory (ADL), and Health Sciences Core Facility (HSCF) for their technical support. The authors also thank Log City Meats LLC in Dundee, NY for providing the porcine aortic valves.

References

1 R. V. Freeman and C. M. Otto, Spectrum of calcific aortic valve disease: pathogenesis, disease progression, and treatment strategies, *Circulation*, 2005, **111**(24), 3316–3326, DOI: 10.1161/CIRCULATIONAHA.104.486738.

2 G. J. Mahler, E. J. Farrar and J. T. Butcher, Inflammatory cytokines promote mesenchymal transformation in embryonic and adult valve endothelial cells, *Arterioscler., Thromb., Vasc. Biol.*, 2013, **33**(1), 121–130, DOI: 10.1161/ATVBAHA.112.300504.

3 N. M. Rajamannan, F. J. Evans, E. Aikawa, K. J. Grande-Allen, L. L. Demer and D. D. Heistad, *et al.*, Calcific Aortic Valve Disease: Not Simply a Degenerative Process A Review and Agenda for Research from the National Heart and Lung and Blood Institute Aortic Stenosis Working Group, *Circulation*, 2011, **124**(16), 1783–1791, DOI: 10.1161/CIRCULATIONAHA.110.006767.

4 S. Dahal, P. Huang, B. T. Murray and G. J. Mahler, Endothelial to mesenchymal transformation is induced by altered extracellular matrix in aortic valve endothelial cells, *J. Biomed. Mater. Res., Part A*, 2017, **105**(10), 2729–2741, DOI: 10.1002/jbm.a.36133.

5 E. J. Benjamin, M. Paul, A. Alvaro, M. S. Bittencourt, C. W. Callaway and A. P. Carson, *et al.*, Heart Disease and Stroke Statistics—2019 Update: A Report From the American Heart Association, *Circulation*, 2019, **139**(10), e56–e528, DOI: 10.1161/CIR.0000000000000659.

6 D. E. Ingber, Developmentally inspired human 'organs on chips', *Development*, 2018, **145**(16), dev156125, DOI: 10.1242/dev.156125.

7 J. T. Butcher, G. J. Mahler and L. A. Hockaday, Aortic valve disease and treatment: The need for naturally engineered solutions, *Adv. Drug Delivery Rev.*, 2011, **63**(4), 242–268, DOI: 10.1016/j.addr.2011.01.008.

8 J. A. Leopold, Cellular Mechanisms of Aortic Valve Calcification, *Circ.: Cardiovasc. Interventions*, 2012, **5**(4), 605–614, DOI: 10.1161/CIRCINTERVENTIONS.112.971028.

9 J. T. Butcher, C. A. Simmons and J. N. Warnock, Mechanobiology of the aortic heart valve, *J. Heart Valve Dis.*, 2008, **17**(1), 62–73.

10 S. Arjunon, S. Rathan, H. Jo and A. P. Yoganathan, Aortic Valve: Mechanical Environment and Mechanobiology, *Ann. Biomed. Eng.*, 2013, **41**(7), 1331–1346, DOI: 10.1007/s10439-013-0785-7.

11 K. Balachandran, P. Sucosky and A. P. Yoganathan, Hemodynamics and Mechanobiology of Aortic Valve Inflammation and Calcification, *Int. J. Inflammation*, 2011, **2011**, 263870, DOI: 10.4061/2011/263870.

12 D. A. Lerman, Calcific Aortic Valve Disease: Molecular Mechanisms And Therapeutic Approaches, *Eur. Cardiol. Rev.*, 2015, **10**(2), 108, DOI: 10.15420/ecr.2015.10.2.108.

13 E. Aikawa and P. Libby, A Rock and a Hard Place: Chiseling Away at the Multiple Mechanisms of Aortic Stenosis, *Circulation*, 2017, **135**(20), 1951–1955, DOI: 10.1161/CIRCULATIONAHA.117.027776.

14 K. L. Sider, M. C. Blaser and C. A. Simmons, Animal Models of Calcific Aortic Valve Disease, *Int. J. Inflammation*, 2011, **2011**, e364310, DOI: 10.4061/2011/364310.

15 D. W. Swinkels and P. N. M. Demacker, Comparative studies on the low density lipoprotein subfractions from pig and man, *Comp. Biochem. Physiol. B Biochem. Mol. Biol.*, 1988, **90**(2), 297–300, DOI: 10.1016/0305-0491(88)90076-4.

16 R. A. Gould and J. T. Butcher, Isolation of Valvular Endothelial Cells, *J. Visualized Exp.*, 2010, **46**, e2158, DOI: 10.3791/2158.

17 S. T. Gould, E. E. Matherly, J. N. Smith, D. D. Heistad and K. S. Anseth, The role of valvular endothelial cell paracrine signaling and matrix elasticity on valvular interstitial cell activation, *Biomaterials*, 2014, **35**(11), 3596–3606, DOI: 10.1016/j.biomaterials.2014.01.005.

18 H. Tseng, L. R. Balaoing, B. Grigoryan, R. M. Raphael, T. C. Killian and G. R. Souza, *et al.*, A three-dimensional co-culture model of the aortic valve using magnetic levitation, *Acta Biomater.*, 2014, **10**(1), 173–182, DOI: 10.1016/j.actbio.2013.09.003.

19 J. Hjortnaes, K. Shapero, C. Goettsch, J. D. Hutcheson, J. Keegan and J. Kluin, *et al.*, Valvular interstitial cells suppress calcification of valvular endothelial cells, *Atherosclerosis*, 2015, **242**(1), 251–260, DOI: 10.1016/j.atherosclerosis.2015.07.008.

20 J. Hjortnaes, G. Camci-Unal, J. D. Hutcheson, S. M. Jung, F. J. Schoen and J. Kluin, *et al.*, Directing Valvular Interstitial Cell Myofibroblast-Like Differentiation in a Hybrid Hydrogel Platform, *Adv. Healthcare Mater.*, 2015, **4**(1), 121–130, DOI: 10.1002/adhm.201400029.

21 T. W. Gee, J. M. Richards, A. Mahmut and J. T. Butcher, Valve endothelial-interstitial interactions drive emergent complex calcific lesion formation in vitro, *Biomaterials*, 2021, **269**, 120669, DOI: 10.1016/j.biomaterials.2021.120669.

22 J. T. Butcher, S. Tressel, T. Johnson, D. Turner, G. Sorescu and H. Jo, *et al.*, Transcriptional Profiles of Valvular and Vascular Endothelial Cells Reveal Phenotypic Differences, *Arterioscler., Thromb., Vasc. Biol.*, 2006, **26**(1), 69–77, DOI: 10.1161/01.ATV.0000196624.70507.0d.

23 J. T. Butcher and R. M. Nerem, Valvular Endothelial Cells Regulate the Phenotype of Interstitial Cells in Co-culture: Effects of Steady Shear Stress, *Tissue Eng.*, 2006, **12**(4), 905–915, DOI: 10.1089/ten.2006.12.905.

24 E. W. K. Young, A. R. Wheeler and C. A. Simmons, Matrix-dependent adhesion of vascular and valvular endothelial cells in microfluidic channels, *Lab Chip*, 2007, **7**(12), 1759–1766, DOI: 10.1039/B712486D.

25 M. B. Chen, S. Srigunapalan, A. R. Wheeler and C. A. Simmons, A 3D microfluidic platform incorporating methacrylated gelatin hydrogels to study physiological cardiovascular cell–cell interactions, *Lab Chip*, 2013, **13**(13), 2591–2598, DOI: 10.1039/C3LC00051F.

26 G. J. Mahler, C. M. Frendl, Q. Cao and J. T. Butcher, Effects of shear stress pattern and magnitude on mesenchymal transformation and invasion of aortic valve endothelial cells, *Biotechnol. Bioeng.*, 2014, **111**(11), 2326–2337, DOI: 10.1002/bit.25291.

27 X. Wang, J. Lee, M. Ali, J. Kim and C. M. R. Lacerda, Phenotype Transformation of Aortic Valve Interstitial Cells Due to Applied Shear Stresses Within a Microfluidic Chip, *Ann. Biomed. Eng.*, 2017, **45**(10), 2269–2280, DOI: 10.1007/s10439-017-1871-z.

28 J. Lee, Z. Estlack, H. Somaweera, X. Wang, C. M. R. Lacerda and J. Kim, A microfluidic cardiac flow profile generator for studying the effect of shear stress on valvular endothelial cells, *Lab Chip*, 2018, **18**(19), 2946–2954, DOI: 10.1039/C8LC00545A.

29 S. G. Mina, W. Wang, Q. Cao, P. Huang, B. T. Murray and G. J. Mahler, Shear stress magnitude and transforming growth factor-βeta 1 regulate endothelial to mesenchymal transformation in a three-dimensional culture microfluidic device, *RSC Adv.*, 2016, **6**(88), 85457–85467, DOI: 10.1039/C6RA16607E.

30 H. Puchtler, S. N. Meloan and M. S. Terry, On the History and Mechanism of Alizarin Red S Stains for Calcium, *J. Histochem. Cytochem.*, 1969, **17**(2), 110–124, DOI: 10.1177/17.2.110.

31 J. M. Richards, J. A. M. R. Kunitake, H. B. Hunt, A. N. Wnorowski, D. W. Lin and A. L. Boskey, *et al.*, Crystallinity of hydroxyapatite drives myofibroblastic activation and calcification in aortic valves, *Acta Biomater.*, 2018, **71**, 24–36, DOI: 10.1016/j.actbio.2018.02.024.

32 C. A. Gregory, W. G. Gunn, A. Peister and D. J. Prockop, An Alizarin red-based assay of mineralization by adherent cells in culture: comparison with cetylpyridinium chloride extraction, *Anal. Biochem.*, 2004, **329**(1), 77–84, DOI: 10.1016/j.ab.2004.02.002.

33 J. Schindelin, I. Arganda-Carreras, E. Frise, V. Kaynig, M. Longair and T. Pietzsch, *et al.*, Fiji: an open-source platform for biological-image analysis, *Nat. Methods*, 2012, **9**(7), 676–682, DOI: 10.1038/nmeth.2019.

34 M. Scimeca, S. Bischetti, H. K. Lamsira, R. Bonfiglio and E. Bonanno, Energy Dispersive X-ray (EDX) microanalysis: A powerful tool in biomedical research and diagnosis, *Eur. J. Histochem.*, 2018, **62**(1), 2841, DOI: 10.4081/ejh.2018.2841.

35 D. Mikroulis, D. Mavrilas, J. Kapolos, P. G. Koutsoukos and C. Lolas, Physicochemical and microscopical study of calcific deposits from natural and bioprosthetic heart valves. Comparison and implications for mineralization mechanism, *J. Mater. Sci.: Mater. Med.*, 2002, **13**(9), 885–889.

36 K. L. Cloyd, I. El-Hamamsy, S. Boonrungsiman, M. Hedegaard, E. Gentleman and P. Sarathchandra, *et al.*, Characterization of Porcine Aortic Valvular Interstitial Cell 'Calcified' Nodules, *PLoS One*, 2012, **7**(10), e48154, DOI: 10.1371/journal.pone.0048154.

37 G. Griffanti, W. Jiang and S. N. Nazhat, Bioinspired mineralization of a functionalized injectable dense collagen hydrogel through silk sericin incorporation, *Biomater. Sci.*, 2019, **7**(3), 1064–1077, DOI: 10.1039/C8BM01060A.

38 P. M. Taylor, Biological matrices and bionanotechnology, *Philos. Trans. R. Soc., B*, 2007, **362**(1484), 1313–1320, DOI: 10.1098/rstb.2007.2117.

39 S. Dahal, J. A. Bramsen, B. R. Alber, B. T. Murray, P. Huang and M.-H. Chen, *et al.*, Chondroitin Sulfate Promotes Interstitial Cell Activation and Calcification in an In Vitro Model of the Aortic Valve, *Cardiovasc. Eng. Technol.*, 2021, DOI: 10.1007/s13239-021-00586-z.

40 M. Rattazzi and P. Pauletto, Valvular endothelial cells: Guardians or destroyers of aortic valve integrity?, *Atherosclerosis*, 2015, **242**(2), 396–398, DOI: 10.1016/j.atherosclerosis.2015.07.034.

41 K. Driscoll, A. D. Cruz and J. T. Butcher, Inflammatory and Biomechanical Drivers of Endothelial-Interstitial Interactions

in Calcific Aortic Valve Disease, *Circ. Res.*, 2021, **128**(9), 1344–1370, DOI: 10.1161/CIRCRESAHA.121.318011.

42 R. F. Ankeny, V. H. Thourani, D. Weiss, J. D. Vega, W. R. Taylor and R. M. Nerem, *et al.*, Preferential Activation of SMAD1/5/8 on the Fibrosa Endothelium in Calcified Human Aortic Valves - Association with Low BMP Antagonists and SMAD6, *PLoS One*, 2011, **6**(6), e20969, DOI: 10.1371/journal.pone.0020969.

43 P. Sucosky, K. Balachandran, A. Elhammali, H. Jo and A. P. Yoganathan, Altered Shear Stress Stimulates Upregulation of Endothelial VCAM-1 and ICAM-1 in a BMP-4– and TGF-β1–Dependent Pathway, *Arterioscler., Thromb., Vasc. Biol.*, 2009, **29**(2), 254–260, DOI: 10.1161/ATVBAHA.108.176347.

44 T. Gaur, C. J. Lengner, H. Hovhannisyan, R. A. Bhat, P. V. N. Bodine and B. S. Komm, *et al.*, Canonical WNT Signaling Promotes Osteogenesis by Directly Stimulating Runx2 Gene Expression, *J. Biol. Chem.*, 2005, **280**(39), 33132–33140, DOI: 10.1074/jbc.M500608200.

45 V. Garg, A. N. Muth, J. F. Ransom, M. K. Schluterman, R. Barnes and I. N. King, *et al.*, Mutations in NOTCH1 cause aortic valve disease, *Nature*, 2005, **437**(7056), 270–274, DOI: 10.1038/nature03940.

46 P. Dutta and J. Lincoln, Calcific Aortic Valve Disease: a Developmental Biology Perspective, *Curr. Cardiol. Rep.*, 2018, **20**(4), 21, DOI: 10.1007/s11886-018-0968-9.

47 B. Jian, N. Narula, Q. Li, E. R. Mohler and R. J. Levy, Progression of aortic valve stenosis: TGF-β1 is present in calcified aortic valve cusps and promotes aortic valve interstitial cell calcification via apoptosis, *Ann. Thorac. Surg.*, 2003, **75**(2), 457–465, DOI: 10.1016/S0003-4975(02)04312-6.

48 K. J. Rodriguez and K. S. Masters, Regulation of valvular interstitial cell calcification by components of the extracellular matrix, *J. Biomed. Mater. Res., Part A*, 2009, **90A**(4), 1043–1053, DOI: 10.1002/jbm.a.32187.

49 N. M. Landry, S. G. Rattan and I. M. C. Dixon, An Improved Method of Maintaining Primary Murine Cardiac Fibroblasts in Two-Dimensional Cell Culture, *Sci. Rep.*, 2019, **9**(1), 12889, DOI: 10.1038/s41598-019-49285-9.

50 D. Bazin, M. Daudon, C. Combes and C. Rey, Characterization and Some Physicochemical Aspects of Pathological Microcalcifications, *Chem. Rev.*, 2012, **112**(10), 5092–5120, DOI: 10.1021/cr200068d.

51 J. Cosmidis, K. Benzerara, N. Nassif, T. Tyliszczak and F. Bourdelle, Characterization of Ca-phosphate biological materials by scanning transmission X-ray microscopy (STXM) at the Ca L2,3-, P L2,3- and C K-edges, *Acta Biomater.*, 2015, **12**, 260–269, DOI: 10.1016/j.actbio.2014.10.003.

52 O. Gourgas, J. Marulanda, Z. Peng, M. Monzur and M. Cerruti, Multidisciplinary Approach to Understand Medial Arterial Calcification, *Arterioscler., Thromb., Vasc. Biol.*, 2018, **38**(2), 363–372, DOI: 10.1161/ATVBAHA.117.309808.

53 A. M. Porras, J. A. Westlund, A. D. Evans and K. S. Masters, Creation of disease-inspired biomaterial environments to mimic pathological events in early calcific aortic valve disease, *Proc. Natl. Acad. Sci. U. S. A.*, 2018, **115**(3), E363–E371, DOI: 10.1073/pnas.1704637115.

54 S. Jana and A. Lerman, Behavior of valvular interstitial cells on trilayered nanofibrous substrate mimicking morphologies of heart valve leaflet, *Acta Biomater.*, 2019, **85**, 142–156, DOI: 10.1016/j.actbio.2018.12.005.